Version of Record: https://www.sciencedirect.com/science/article/pii/S0926337319306915
Manuscript_711a59800f57adb66df433416d142c0f

Catalytic C-O bond hydrogenolysis of tetrahydrofuran-dimethanol over Metal supported WO_x/TiO_2 catalysts

Jiayue He,[1] Samuel P. Burt,[1,2], Madelyn R. Ball,[1] Ive Hermans,[1,2] James A. Dumesic,[1] George W. Huber[1*]

[1.]Department of Chemical and Biological Engineering, University of Wisconsin-Madison, Madison, WI 53706, USA. [2.]Department of Chemistry, University of Wisconsin-Madison, Madison, WI 53706, USA.

Corresponding authors: gwhuber@wisc.edu;

Abstract

M-WO_x/TiO_2 (M = Pt-, Rh-, Pd-, and Ru) catalysts were prepared and studied for tetrahydrofuran-dimethanol (THFDM) hydrogenolysis. All catalysts have a small metal particle size (< 2 nm) but show catalytic activities that differ by two orders of magnitude. From a combination of CO chemisorption and STEM, we conclude that this wide gap in activity is primarily due to overgrowth of WO_x/TiO_2 covering the metal particle of the less-active catalysts. This overgrowth decreases the number of exposed hydrogenation sites in these catalysts, lowering the overall reaction rate. The catalyst with the highest activity (Pt-WO_x/TiO_2) was studied at various pressures of H_2, with catalytic activity passing through a maximum with increasing pressure. This increase is likely due to changes in the oxidation state of $W^{\delta+}$ on the catalyst surface, which changes from W^{6+} to W^{5+} and W^{4+} with increasing hydrogen pressure. The apparent activation energy of THFDM conversion over Pt-WO_x/TiO_2 is 47 $kJ \cdot mol^{-1}$. Pt-WO_x/TiO_2 showed a decrease in conversion from 45% to 22% over 45 hours on stream in a continuous flow reactor. Catalyst deactivation is likely due to leaching of W. THFDM can be efficiently converted to 1,2,6-hexanetriol in the presence of Pt/TiO_2 and homogeneous W salts.

1.0 Introduction

Cellulose derived from lignocellulosic biomass is the most abundant renewable carbon resource in nature, making it a promising feedstock for the production of bio-based chemicals. [1–5]1,6-Hexanediol (1,6-HDO) is a high value chemical with a market price of $4,400/ton, an annual market size of 138,000 tons, and a global market value of approximately $600 MM.[6] It is primarily used as a monomer for polyesters and polyurethanes.[7] The most common industrial route for 1,6-HDO production begins with naphtha cracking to benzene, which is then hydrogenated to cyclohexane, which can be oxidized to a mixture of cyclohexanol and cyclohexanone (KA oil).[8,9] KA oil can then be further oxidized to adipic acid or its esters, which are finally hydrogenated to 1,6-HDO.[7–11] This traditional route suffers from low single pass conversions, homogeneous chemistry, excess use of HNO_3 which leads to the production of N_xO_y, and the nonrenewable use of petroleum-based feedstocks. It would be desirable to develop a new route to 1,6-HDO from renewable lignocellulosic feedstocks.

© 2019 published by Elsevier. This manuscript is made available under the Elsevier user license
https://www.elsevier.com/open-access/userlicense/1.0/

Several academic and industrial groups have studied the production of 1,6-HDO from cellulose-derived feedstocks. Each route studied appears to pass through the common intermediate tetrahydrofuran-dimethanol (THFDM).[12] Hydrogenolysis of THFDM to 1,6-HDO, therefore, is of importance to the production of 1,6-HDO from cellulose. In 1981, Faber showed THFDM hydrogenolysis over a copper chromite catalyst, but 1,6-HDO yields were not reported.[13] Buntara *et al.* reported a one-pot conversion of THFDM to 1,6-HDO using a combination of Rh-ReO_x/SiO_2 and Nafion SAC-13 with 1,6-HDO yields up to 86%.[14,15] This process suffers from low catalyst activity (0.10 mol·mol $_{Rh}^{-1}$ ·min^{-1} with THFDM conversion of 21% at 80 °C) and rapid catalyst deactivation, primarily due to high solubility of the SiO_2 support in the solvent, water.[14,15] Rh-ReO_x, as well as base metal catalysts, have been extensively studied for the conversion of tetrahydropyran-2-methanol (THP-2M) to 1,6-HDO,[16–18] but they have not been shown to be active for the one-step conversion of THFDM to 1,6-HDO. As shown previously and again here in **Scheme 1**, THP-2M is an intermediate between THFDM and 1,6-HDO.[12] Most recently, Rennovia, Dupont, and our group have reported a process to convert THFDM to 1,6-HDO over a Pt-WO_x/TiO_2 catalyst with 1,6-HDO yields over 70%.[12,19,20] Using a combination of Raman spectroscopy, X-ray Photoelectron Spectroscopy (XPS), and CO chemisorption, it was determined that H_2 spillover from the Pt nanoparticle to WO_x was effective in reducing W^{6+} to W^{5+}, generating a Brønsted acid site that is active for activation of the C-O bond to open the ring of THFDM.[12] This spillover was possible even in the absence of direct contact between WO_x and Pt, due to the reducible nature of TiO_2 facilitating H atom transfer over the catalyst surface over distances on the order of micrometers from the Pt particle.[12,21]

In our previous paper, we showed that the role of Pt was to dissociate H_2 and provide hydrogenation sites.[12] The objective of this paper is to investigate the role of different noble metals, H_2 pressure, reaction temperature, and homogeneous tungsten salts on THFDM hydrogenolysis. We have also observed that the TOF of 10 wt.% Pt-WO_x/TiO_2 are higher than the TOFs of 4 wt.% Pt-WO_x/TiO_2. Therefore, a 10 wt.% Pt is used in this study.[12]We first investigate whether this high reactivity for THFDM hydrogenolysis is specific to Pt-WO_x/TiO_2 or if other metals commonly used for hydrogenations (Rh, Pd, Ru) can be substituted for Pt as a hydrogenation catalyst, while maintaining similar reactivity or even improving it.[22–24] We then use XPS, STEM, and CO chemisorption to investigate the cause for the reactivity trends we see in these catalysts. Next, we study the effect of temperature on reactivity, and calculate an activation energy for THFDM conversion. We use XPS to help explain our reactivity trends. We then study the most active catalyst in a fixed-bed reactor and investigate causes of deactivation.

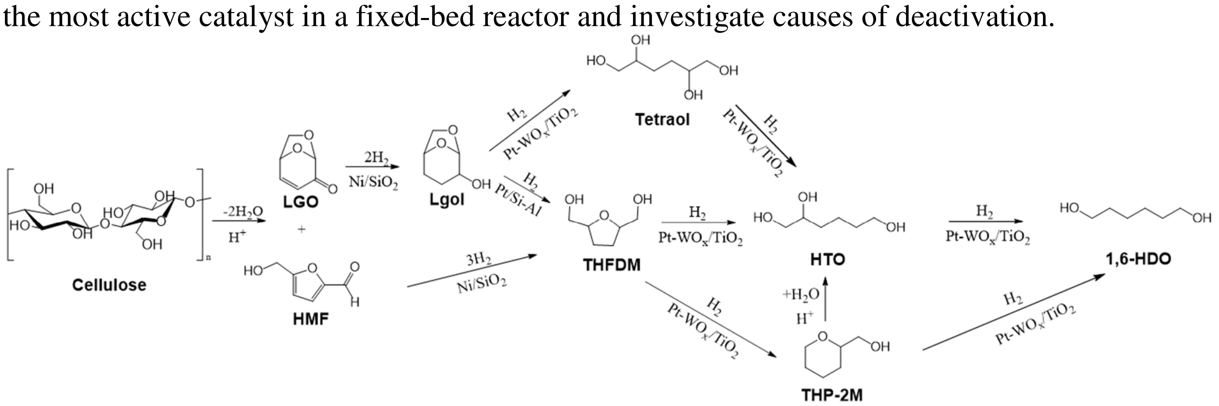

Scheme 1. Proposed reaction pathway for the conversion of cellulose derived oxygenates.[12,25–29]

2.0 Experimental

2.1 Catalytic reactions

2.1.1 Cellulose derived cyclic ethers conversion in a batch reactor

Reactions were performed in 50 mL HEL high-pressure batch reactors. Prior to reactions, the catalysts were activated under flowing H_2 (100 mL (STP) min^{-1}) (Airgas, UHP) at 250˚C for two hours (1 ˚C min^{-1}). The reactant solution in water (Fisher Scientific #11307090) was then pumped into the reactor. The reactor was purged three times with H_2 prior to reaction, pressurized to the desired H_2 pressure, stirred at 700 rpm, and heated to the reaction temperature. After reaction, the reactor was cooled in ice water and depressurized. The effect of the stirring rate was carefully evaluated. It is found that the reaction rates/ conversions are the same when the stirring rate is above 400 rpm. Therefore, there are no external transport limitations under our reaction conditions (700 rpm). The product mixture was then filtered using a 0.22 μm PES (polyethersulfone) syringe filter.

Products were quantified with a Shimadzu Gas Chromatograph using a Flame Ionization Detector (FID) with liquid injection. A Restek RTX-VMS capillary column (Length: 30 m, ID: 0.25 mm, film thickness: 1.4 μm) was used. The FID response factor of unknown products with retention times close to that of 1,2-hexanediol was assumed to be equal to that of 1,2-hexanediol. Based on this assumption, the carbon balance was calculated to be 95%±5% in all experiments.

2.1.2 Cellulose derived cyclic ethers conversion in continuous flow reactor for stability test

Hydrogenolysis was carried out in a grade 316 stainless-steel tubular flow reactor (30 cm long, 6.35 mm outer diameter) arranged in an upflow configuration and heated using a tube furnace (Thermcraft Inc. No. 114-12-1ZH). The catalyst (0.10 g), without dilution, was added into the reactor with quartz wool and quartz beads packed on both sides. The catalyst without dilution was reduced under a H_2 flow (100 mL (STP) min^{-1}) at 250˚C for 2 h before reaction. The reactor was cooled to 160˚C and pressurized to 3.4 MPa H_2. An aqueous 1 wt% THFDM solution was pumped into the reactor at 0.04 mL/min using an Agilent Prostar HPLC pump with co-fed H_2 (40 mL (STP) min^{-1}). Two stainless steel tanks (150 cm^3 each) were used to accumulate the liquid products at the reactor outlet. The accumulated liquid product was drained periodically into a collector container, filtered through a 0.22 μm PES syringe filter, and then analyzed by GC. The carbon balance in the first 10 hours was poor, indicating that this time was required to achieve steady state, therefore data is only reported after 10 hrs time on stream. The gaseous products continued to flow through a back-pressure regulator to maintain the reaction pressure. Both an excess flow shut-off valve and a pressure relief valve were also installed in the reactor system to ensure safe operation. The feed solutions and the liquid products were analyzed using a gas chromatograph (Shimadzu, GC-2010) equipped with a flame ionization detector (FID) and a Restek RTX-VMS capillary column. The gas effluent from the continuous flow reactor was analyzed using a gas chromatograph (Shimadzu, GC-2014) equipped with an FID and a Restek RT-Q-Bond capillary column as well as a thermal conductivity detector and a ShinCarbon ST micropacked column.

2.2 Catalyst synthesis

2.2.1 WO_x/TiO_2 supports synthesis

WO_x/TiO_2 supports was synthesized by wet impregnation of ammonium tungsten oxide hydrate (Alfa Aesar #22640) on TiO_2 nanopowder (Sigma-Aldrich #718467). Ammonium tungsten oxide hydrate was first added to 100 mL of 18 MΩ water. To dissolve the tungsten precursor, HCl (Sigma-Aldrich #258148) was added dropwise to the mixture until it reached a pH of 1, and the mixture was then heated under reflux to 80 ˚C for 12 hours. 6 g of TiO_2 nanopowder were then added to the mixture and left to stir for an additional 30 minutes at 80 ˚C. Water was then evaporated by rotary evaporation using a water bath at 60 ˚C. WO_x/TiO_2 powders were then dried at 110 ˚C overnight and calcined under flowing air at 400 ˚C for three hours (1 ˚C min^{-1}).

2.2.2 M-WO_x/TiO_2 and M/TiO_2 catalysts synthesis

All the catalysts were synthesized with similar procedures. For example, Pt-WO_x/TiO_2 catalysts were synthesized by wet impregnation of chloroplatinic acid (Sigma-Aldrich # 262587) on synthesized WO_x/TiO_2 and TiO_2 supports. (The precursors for Ru-, Rh-, and Pd-WO_x/TiO_2 are ruthenium (III) chloride (Sigma-Aldrich #208523), rhodium (III) nitrate hydrate (Sigma-Aldrich #83750) and palladium (II) nitrate dihydrate (Sigma-Aldrich #76070), respectively.) A chloroplatinic acid solution in water was added to the WO_x/TiO_2 support. The mixture was then heated to 80 ˚C while stirring. The mixture was then dried at 80 ˚C in vacuum oven overnight. The dry solid was ground to a powder. The powder was then calcined under flowing air (Airgas, UHP, 100 mL min^{-1}) at 400 ˚C for three hours (1 ˚C min^{-1}) and subsequently reduced under flowing H_2 (Airgas, UHP, 100 cm^3(STP) min^{-1}) at 250 ˚C for two hours (1 ˚C min^{-1}). After cooling to room temperature, the catalysts were passivated under flowing 1% air in He (Airgas, UHP) or transferred and stored in a glovebox.

2.3 Catalyst Characterization

2.3.1 Inductively Coupled Plasma-Atomic Emission Spectroscopy (ICP-AES)

The solid samples were digested in a mixture of HCl (Sigma-Aldrich #258148), HNO_3 (Sigma-Aldrich #438073), and HF (Sigma-Aldrich #339261) at 120 ^oC overnight. The elemental compositions of the synthesized samples were analyzed by ICP-OES (Varian Vista-MPX CCD Simultaneous ICP-OES). Metal standards for the ICP analysis were prepared from Fluka (1000 ± 2 mg/L).

2.3.2 N_2 physisorption measurements

N_2 physisorption measurements were measured on a Micromeritics 3Flex apparatus. The samples were degassed prior to measurement for 4 h at 150 ^oC under vacuum. Adsorption isotherms were collected at -196.15 ^oC and analyzed using the BET method.

2.3.3 X-ray Photoelectron Spectroscopy (XPS)

Surface compositions were characterized by X-ray Photoelectron Spectroscopy (XPS) using a K-alpha XPS (Thermo Scientific) instrument with a micro-focused monochromatic Al Kα X-ray source. Prior to analysis, the catalysts were reduced with flowing H_2 at 250˚C for two hours (1 ˚C min^{-1}), and stored in an oxygen-free environment, where they could be loaded in an air-tight sample holder for transport to the spectrometer. When it was desired to analyze oxidized samples, catalysts were treated in 1% O_2/N_2 at room temperature after reduction, and the same process was carried out. The samples were analyzed at 10^{-7} mbar pressure and room temperature. The spectra in the C1s, O1s, Pt4f, W4d, and Ti2p regions were collected over multiple scans; the number of scans was adjusted for each element (C = 15, O = 20, Pt = 60, W = 60, Ti = 20) to obtain an acceptable signal/noise ratio. The pass energy was held at 50 eV, the dwell time at 50 ms, and the energy step size at 0.2 eV for each region. Each region was integrated using the Avantage (Thermo Scientific) software package for determination of surface composition.

2.3.4 CO Chemisorption

CO Chemisorption measurements were carried out with a Micromeritics Autochem II Chemisorption Analyzer. Approximately 100 mg of sample was used for each measurement. Prior to CO chemisorption, samples were reduced under 40 mL (STP) min^{-1} 10%H_2/Ar (Airgas) to 250 ˚C (1 ^{o}C min^{-1}) for two hours. Samples were then cooled to 35˚C under 10 mL (STP) min^{-1} He (Airgas, UHP) flow. 5%CO/He (Airgas) was then pulsed onto the catalyst in 0.5 mL (STP) increments until consecutive signals were equal. Signals were then integrated to determine total CO consumption.

2.4 THFDM synthesis

HMF (Hefei leaf biotech, 12.0 g), the solvent (120 mL ethanol, Decon Laboratories, INC.) and Ni/SiO_2 (64 wt.%, Strem #28-1900, 1.20 g) were added to a 300 mL Hastalloy Parr autoclave. The reactor was flushed three times with hydrogen and pressurized to 8 MPa. The reaction mixture was stirred at 700 rpm and heated to 80 ˚C for 6 hrs. The autoclave was then allowed to cool to ambient temperature and the pressure was released. The obtained mixture was first filtered with a 0.22 μm PTFE (polytetrafluoroethylene) syringe filter to remove Ni/SiO_2. The solvent ethanol was evaporated with rotary evaporation using a water bath of 80 ˚C. The obtained liquid (THFDM) was analyzed by GC and 13C NMR (**Fig. S4**). [12]

The product from HMF hydrogenation was characterized with ^{13}C NMR. The sample was rotary evaporated to remove the ethanol solvent and dissolved in D_2O. The NMR experiments were carried out using a Bruker Biospin (Billerica,MA) AVANCE III 500 MHz spectrometer fitted with a DCH (^{13}C-optimized cyroprobe). The ^{13}C experiments were run with the Bruker standard pulse sequence 'zgig30' with 128 scans of 65,786 data points at a 1 s acquisition time, a 12 s inter-scan relaxation delay, and a 262 ppm sweep width centered at 100 ppm. MestReNova software was used to process the spectra and the spectra were referenced to the residual water peak at 4.79 ppm.

3.0 Results and discussion

3.1 THFDM Conversion over M-WO_x/TiO_2 catalysts

Fig. 1 shows the product distribution for THFDM conversion over the four bimetallic catalysts used in this study. **Fig. 1(a&b)** show that Pd- and Ru-WO_x/TiO_2 exhibit low activity for this reaction, whereas the Pt and Rh-WO_x/TiO_2 have higher activities. This behavior is similar to the study of Amada *et al.*, who observed that Pd-ReO_x/SiO_2 exhibits almost no activity for glycerol hydrogenolysis at 100 °C.[30] Tomishige *et al.* also reported that the promoting effect of oxophilic Re on Ru is different from the effect of Re on Rh or Ir.[31] The oxophilic additive can, in some cases, cover the metal nanoparticle, thereby decreasing activity of the bimetallic catalyst.[32] **Figure 1** indicates that this behavior could be the case for Pd- and Ru-WO_x/TiO_2, which will be discussed in more detail later. **Figure 1** shows that Ru- and Pt-WO_x/TiO_2 exhibit >98% selectivity to 1,2,6-hexanetriol (HTO), which can then be selectively converted to 1,6-HDO, as shown in our previous paper.[12] Rh-WO_x/TiO_2 displays 80-85% HTO selectivity with THP-2M as the main byproduct.[16,17,32] Pd-WO_x/TiO_2 shows less than 40% selectivity to HTO. However, this catalyst achieves a combined selectivity of ~80% to 1,6-HDO and its precursors.

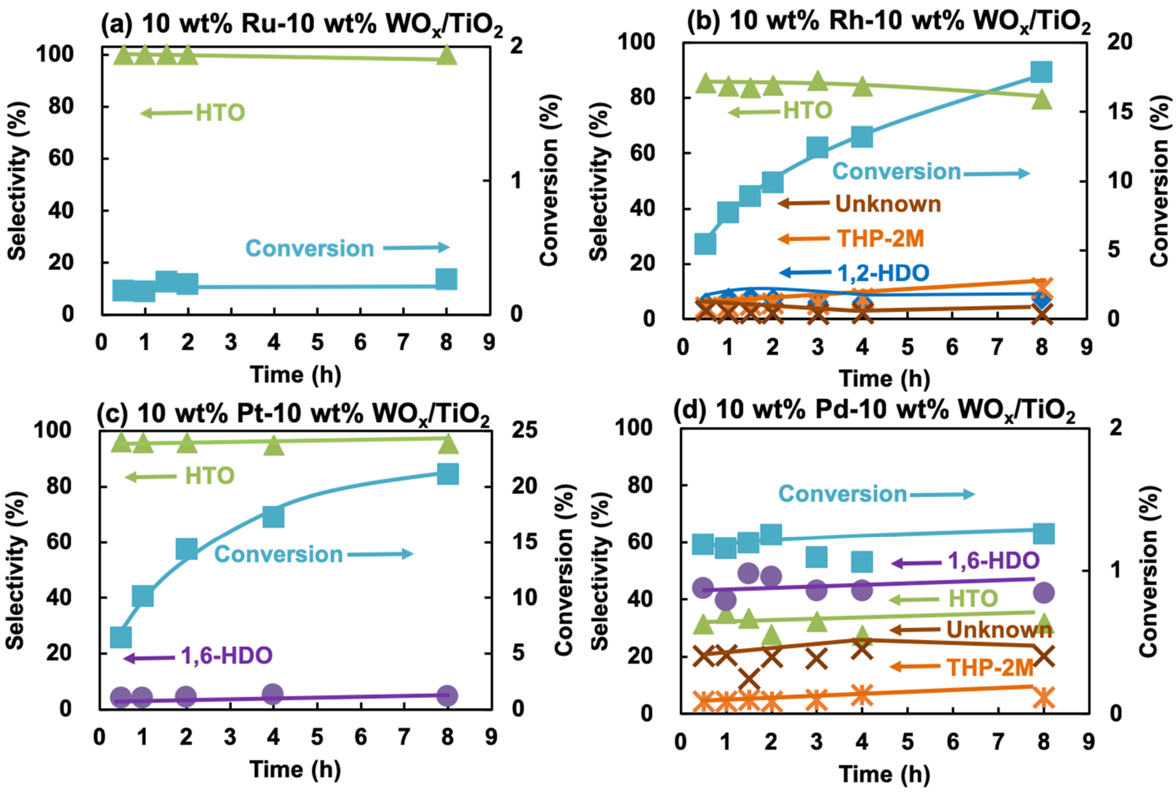

Figure 1. THFDM (5 wt% in H_2O, 20 mL) conversion over 10 wt% metal-10 wt% WO_x/TiO_2 catalysts (0.10 g) at 160°C under 5.5 MPa H_2. (a) 10 wt% Ru-10 wt% WO_x/TiO_2 (b) 10 wt% Rh-10 wt% WO_x/TiO_2 (c) 10 wt% Pt-10 wt% WO_x/TiO_2 (d) 10 wt% Pd-10 wt% WO_x/TiO_2.

Fig. 2 shows STEM images of Pt-, Rh-, Pd-, and Ru-WO_x/TiO_2 catalysts prepared in this study. STEM images of monometallic catalysts can be found in the supporting information. The average metal particle sizes of the Pt, Rh, and Pd catalysts range from 1.45 to 1.74 nm. Ru-WO_x/TiO_2 has a smaller average particle size of 0.63 nm. These small particles are typical for noble metals and align with other reported metal-tungsten catalysts in the literature.[33–39] Such high loading metal catalysts have been reported to have larger particles, however, particles are usually smaller than 5 nm for these noble metals[40]. **Table 1** shows average particle sizes determined by STEM, along with CO uptake, CO uptake derived particle sizes, and TOFs for THFDM conversion. The particle sizes determined by STEM of Pt-, Rh-, Ru-, Pd-WO_x/TiO_2 are smaller than the particle size calculated from CO chemisorption, particularly for the Pd and Ru catalysts (**Entry 1-4, Table 1**). Since CO does not adsorb on WO_x/TiO_2, this indicates that the noble metal particles may be overcoated by WO_x to some extent. There is a monolayer of WO_x (around 10 wt.% loading) on TiO_2 surface (**Scheme S1**) since WO_x/TiO_2 is synthesized by first impregnating WO_x on TiO_2. The Pt is then impregnated on WO_x/TiO_2, so there is likely little contact between metal nanoparticles and TiO_2. Ru- and Pd-WO_x/TiO_2 (36 and 5 μmol g^{-1}) have less than half of the CO uptake as Pt- (85 μmol g^{-1}) and Rh-WO_x/TiO_2 (99 μmol g^{-1}), even though STEM images show that Pd-(1.45 ± 1.53 nm) and Ru-WO_x/TiO_2 (0.63 ± 0.66 nm) have similar average particle sizes to the other two bimetallics (1.74 ± 0.78 nm for Pt and 1.51 ± 0.44 nm for Rh) of this study. This result shows that the oxophilic additive (WO_x, in this case) covers more metal sites with the Pd- and Ru-WO_x/TiO_2 catalyst than the Pt- (85 μmol g^{-1}) and Rh-WO_x/TiO_2 catalyst [32]. We note there is uncertainty in the particle size measurements due to the small area of the catalyst which is sampled. However, the difference between measured particle size and estimated particle size from CO chemisorption for the Ru- and Pd-WO_x/TiO_2 catalysts is much larger than what would be accounted for by error in the particle size measurements. Therefore, the low CO uptake on these catalysts is likely due to an overcoat by either WO_x or TiO_2.

Additionally, a similar phenomenon is observed on Pt-, Rh-, Ru-, and Pd/TiO_2; the STEM determined particle sizes are generally smaller than the CO-chemisorption determined ones (**Entry 5-8, Table 1**). On these M-TiO_2 catalysts, the TiO_2 can also overcoat the metal nanoparticles. The particle sizes determined by STEM of Ru- and Pd/TiO_2 are much smaller than the particle size calculated from CO chemisorption (**Entry 5-6, Table 1**). Since the CO does not adsorb on TiO_2, this suggests that the noble metal particles are overcoated by TiO_2. According to the literature [41–45] as the reduction temperature is increased from 200°C to 500 °C, the quantity of adsorbed hydrogen decreases due to metal overcoating of TiO_2. The higher the reduction temperature, the higher this strong metal-support interaction. According to our TEM data and CO chemisorption, all four noble metals were coated by migrating clusters of the support oxide (TiO_2) at 250 °C in a manner similar to SMSI [43,46–49]. These thin TiO_x layers form on the metal particles, physically blocking the interaction of the CO gas molecules with their surface. Our data also show that Pd and Ru nanoparticles have more overcoating than Pt and Rh nanoparticles. According to literature [41,42,46,48], Pt and Rh exhibit very similar behaviors with TiO_2, while Ru tends to have more oxide overcoats than other noble metals. Additionally, it has been reported that TiO_2 overcoats on Pd are feasible at temperatures as low as 350°C[36].

Table 1 reports the analogous data for monometallic Pt-, Rh-, Pd-, and Ru/TiO_2, which shows a similar trend. Each monometallic catalyst has a similar particle size as determined by STEM, but CO uptake is one or two orders of magnitude lower for Ru/TiO_2 (32 μmol g^{-1}) and Pd/TiO_2 (38 μmol g^{-1}) compared to Pt/TiO_2 (177 μmol g^{-1}) and Rh/TiO_2 (201 μmol g^{-1}). We also studied Ru/TiO_2 and Pd/TiO_2 with CO chemisorption with a reduction temperature of 400 °C instead of our normal 250 °C treatment. Ru/TiO_2 had a marginal increase in CO uptake with the increased reduction temperature (from 5 to 7 μmol g^{-1}). Pd/TiO_2 showed a slight decrease in CO uptake from 38 to 36 μmol g^{-1} with the 400 °C reduction temperature. Temperature programmed reduction and XPS experiments also suggest that the low CO uptake for these catalysts is not due to a difficult-to-reduce mixed oxide phase **(Figures S5 and S6)** [50–54]. These data indicate that the Ru and Pd catalysts show low CO uptakes and activities due to the reduced metal being overcoated by TiO_2 in M-TiO_2 or WO_x/TiO_2 in M-WO_x/TiO_2.

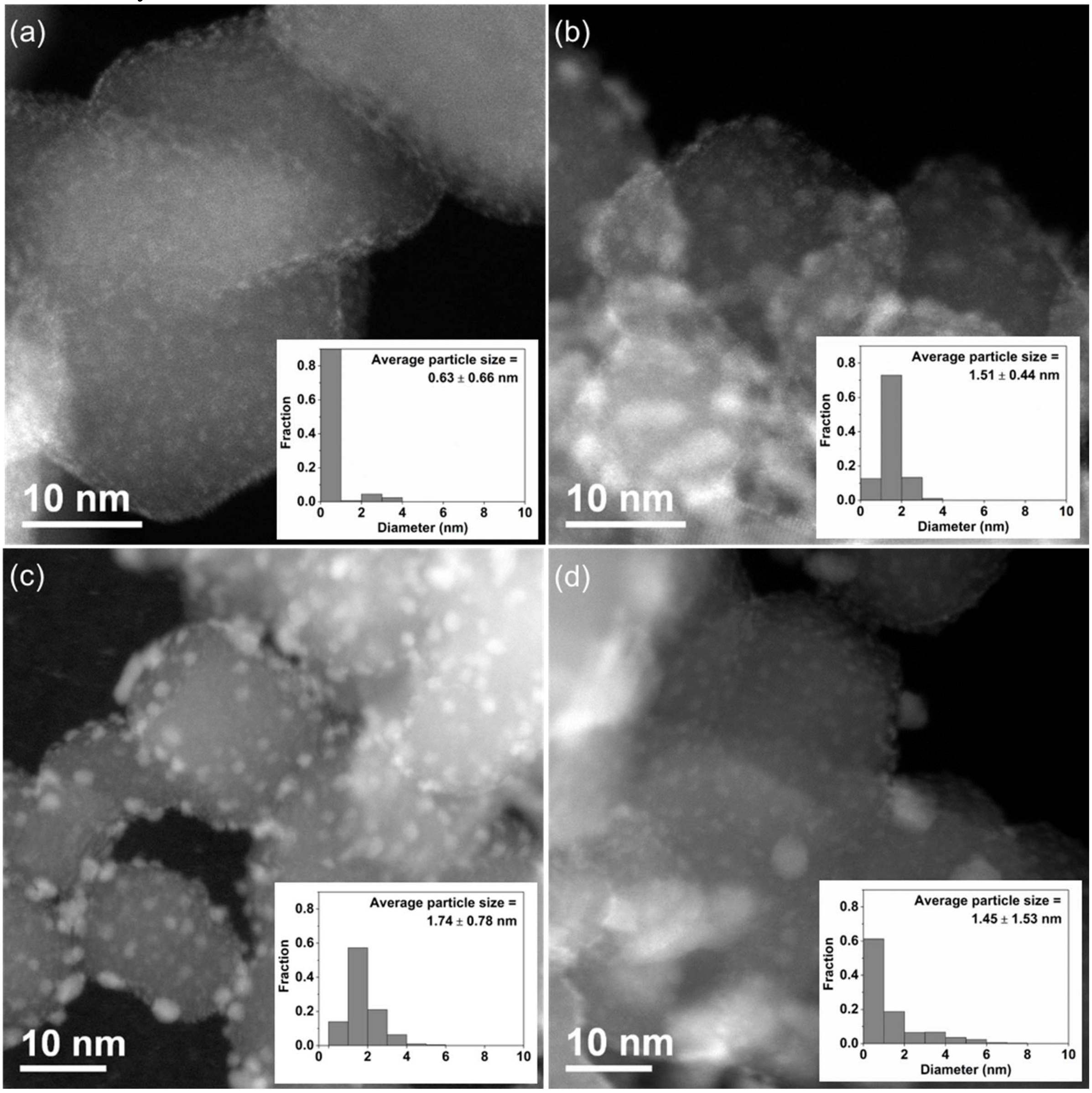

Figure 2 STEM images of (a) 10 wt% Ru-10 wt% WO_x/TiO_2 (b) 10 wt% Rh-10 wt% WO_x/TiO_2 (c) 10 wt% Pt-10 wt% WO_x/TiO_2 (d) 10 wt% Pd-10 wt% WO_x/TiO_2.

Table 1 Properties of M-WO_x/TiO_2 (M=Pt, Pd, Rh, Ru) and Pt/TiO_2 catalysts.

Catalyst	STEM particle size (nm)	Estimated particle size from	CO uptake (μmol g^{-1})	TOF for THFDM conversion	TOF for THFDM conversion

		CO uptake \ (nm)[a]		**(mol·mol $_M^{-1}$ min^{-1})[b]**	**(mol·mol $_{Surf\,M}^{-1}$ min^{-1})[c]**
Pt-WO_x/TiO_2	1.74 ± 0.78	6.2	85	0.29	1.60
Rh-WO_x/TiO_2	1.51 ± 0.44	9.0	99	0.16	1.34
Pd-WO_x/TiO_2	1.45 ± 1.53	26.1	36	0.034	0.80
Ru-WO_x/TiO_2	0.63 ± 0.66	191.9	5	0.0059	0.85
Pt/TiO_2	1.59 ± 0.38	2.8	177	0.044	0.11
Rh/TiO_2	1.37 ± 0.33	5.3	201	0.082	0.40
Pd/TiO_2	1.13 ± 0.89	24.2	38	0.003	0.065
Ru/TiO_2	3.51± 1.16	183	32	0	0

a. The estimated particle size was calculated according to the method.[55] This assumes 100% reduction of the metal and no overcoating of the metal particle.
b. TOF is normalized by the total metal atoms.
c. TOF is normalized by the surface metal atoms.

3.2 Characterization of M-WO_x/TiO_2 by X-Ray Photoelectron Spectroscopy

Fig. 3a shows the W 4d XPS data for each M-WO_x/TiO_2 catalyst after being reduced under H_2 flow at 250 °C for 2 hours. As we have shown in our previous paper, Pt-WO_x/TiO_2 displays mainly W^{5+} and W^{6+} under these reduction conditions.[12] Furthermore, we concluded that the creation of this W^{5+} site during reduction corresponded with the production of a W-OH site, which was active for C-O bond activation in THFDM.[12] There is another signal centered at 283.8 eV in each spectrum which is assigned to the $4d_{5/2}$ electron of W^{4+}.[56] **Fig. 3a** shows that Pt-WO_x/TiO_2 has the highest percentage of W^{5+} compared to the other catalysts. **Fig. 3b** shows that there is a correlation for these four catalysts between the reaction rate for THFDM conversion and the percentage of W^{5+} in the catalysts. The THFDM conversion rate increases with increasing W^{5+} in catalysts (**Fig. 3b**). Besides the positive correlation between percentage of W^{5+} and reactivity, it is also noted that there is a negative correlation between the percentage of W^{4+} and the catalytic activity. It has been previously reported that, for Pt/WO_x catalysts, H atoms become protons and electrons when in contact with the WO_3. The electrons reduce W^{6+} cations to W^{5+} cations and move through the WO_3 lattice by W^{5+}– W^{6+} exchange. Therefore, W^{5+}– W^{6+} exchange is important for the high activity of catalysts. [57,58] It has also been reported that the catalytic redox cycle of W^{6+} - W^{5+} produces the active site in Pt-WO_x/TiO_2 for C-O hydrogenolysis of glycerol, and the over-reduction of W^{5+} to the inactive W^{4+}species decreases activity [33].b

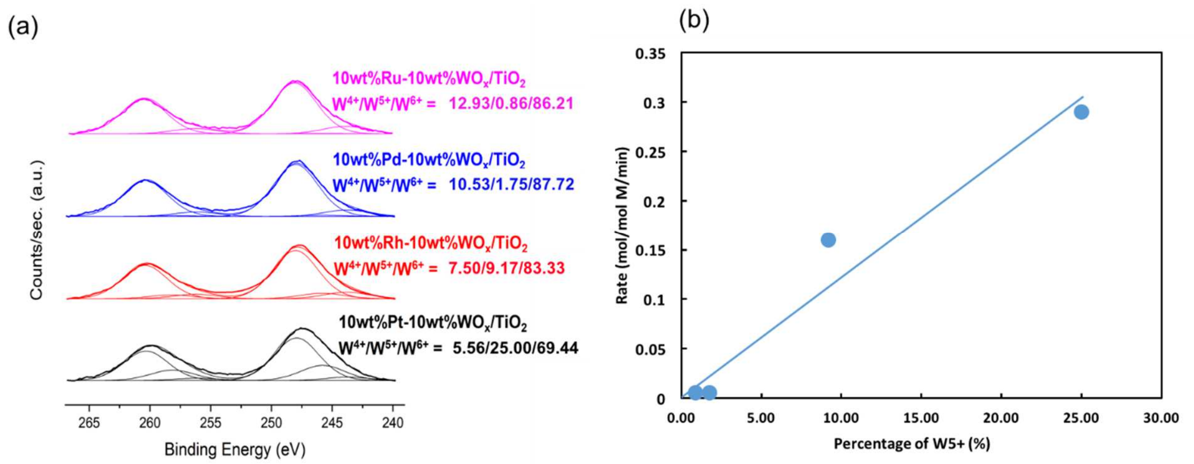

Figure 3. (a) W 4d XPS of M-WO_x/TiO_2 catalysts after reduction under flowing H_2 at 250 ^oC (1 ^oC/min) for 2 hours. (b) THFDM conversion rate versus percentages of W^{5+}in the catalysts.

3.3 Temperature effects of THFDM conversion over Pt- WO_x/TiO_2

Figure 4 shows the effect of reaction temperature on THFDM conversion for the Pt-WO_x/TiO_2 catalyst. The THFDM conversion rate increases from 0.29 mol·mol$_{Pt}^{-1}$· min^{-1} at 160 ˚C to 0.54 mol·mol$_{Pt}^{-1}$· min^{-1} at 180 ˚C to 0.88 mol·mol$_{Pt}^{-1}$· min^{-1} at 200 ˚C. Higher temperatures also lead to higher selectivity to secondary products (1,6-HDO and 1,2-HDO). However, **Figure 4** shows that HTO hydrogenolysis over Pt-WO_x/TiO_2 favors 1,6-HDO, our desired final product, over the less-desirable 1,2-HDO. 1,6-HDO selectivity increases from 4.5% at 160 ˚C to 6% at 180 ˚C to 15% at 200 ˚C, while 1,2-HDO selectivity increases from 0% at 160 ˚C to 3.3% at 180 ˚C to 4% at 200 ˚C (**Fig. 4**). The apparent activation energy for THFDM conversion is calculated to be 47 kJ·mol^{-1} (**Fig. 5**).

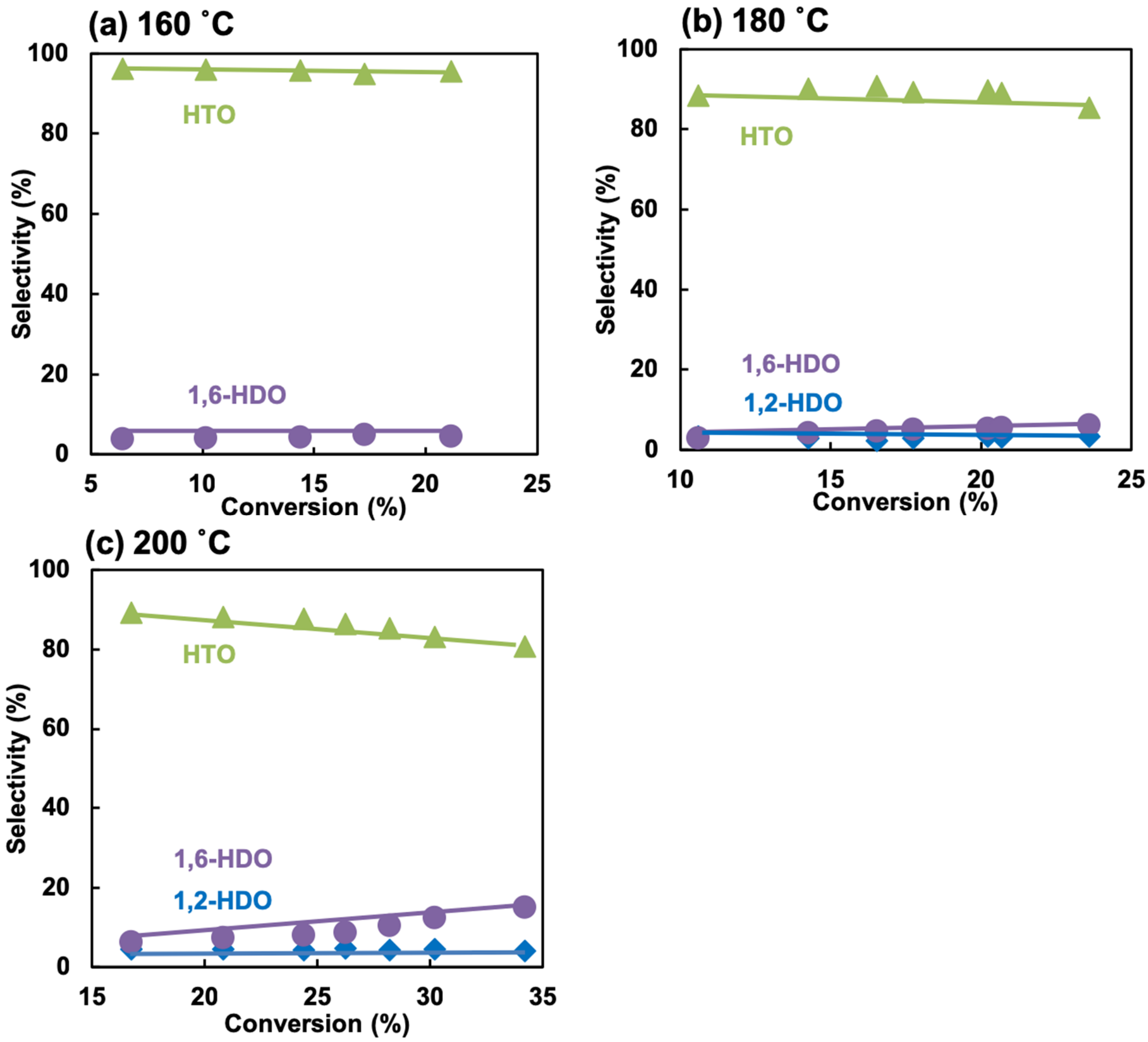

Figure 4 THFDM (5 wt% in H_2O, 20 mL) conversion and product selectivity over 10 wt% Pt-10 wt% WO_x/TiO_2 (0.10 g) catalysts under 5.5 MPa H_2 at (a) 160 ˚C (b) 180 ˚C (c) 200 ˚C.

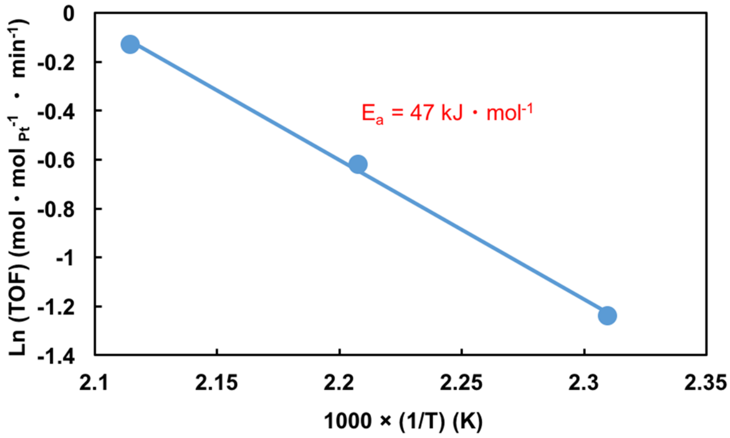

Figure 5. Arrhenius plot for THFDM conversion. Reaction conditions: THFDM (5 wt% in H_2O, 20 mL), 0.10 g 10 wt% Pt-10 wt% WO_x/TiO_2 under 5.5 MPa H_2.

3.4 H_2 pressure effect of THFDM hydrogenolysis over Pt- WO_x/TiO_2

The effect of reaction pressure on THFDM conversion is shown in **Fig. 6**. **Fig. 6a and 6b** show that THP-2M selectivities of up to 30% are achieved at low reaction pressures and low conversions. No THP-2M is observed at pressures of 3.4 and 5.5 MPa, with HTO being the primary product (**Fig. 6a** and **6b**). As shown in **Fig. S2**, the HTO selectivity increases gradually from 70% at 1.0 MPa to 95% at 5.5 MPa H_2, while the THP-2M selectivity decreases from 16% at 1.0 MPa to 0% at 3.4 MPa H_2. This result supports **Scheme 1** which shows that there are two pathways for conversion of THFDM into HTO. The first pathway is through THP-2M while the second pathway involves direct conversion of THFDM into HTO. Both of these pathways first involve a ring opening of the THFDM by a hydrogenolysis step which likely involves an oxocarbenium ion.[16] HTO is likely formed from hydrogenation of this oxocarbenium ion, while THP-2M is likely formed by a ring closing dehydration of the oxocarbenium ion followed by hydrogenation (see proposed reaction pathway in **Scheme S2**). **Fig. 6e** shows that the THFDM conversion rate passes through a maximum of 0.45 mol·mol$_{Pt}^{-1}$·min^{-1} at 2.0 MPa, then gradually decreases to 0.29 mol·mol$_{Pt}^{-1}$·min^{-1} at 5.5 MPa.

Fig. 7 shows the XPS of the Pt/WO_x-TiO_2 catalyst as a function of hydrogen pressure. **Fig. 7a** shows the Pt 4f region of Pt-WO_x/TiO_2 after reduction at various H_2 pressures at 250 °C. This data indicates that H_2 pressure does not change the oxidation state of Pt. **Fig. 7b** shows the W 4d region of each of these catalysts. We can see that the H_2 pressure used during reduction has a strong effect on the W oxidation state. Specifically, we see that the amount of W^{4+} and W^{5+} relative to W^{6+} increases with increasing reduction pressure. This behavior agrees with the studies of Wang *et al.*, in which they also observed maximum activity at an intermediate H_2 pressure for glycerol hydrogenolysis with Pt/WO_x[33]. The lower activity at higher H_2 pressure was partly attributed to the further reduction of W^{5+} to W^{4+}[33]. According to **Fig.7b**, the percentage of W^{4+} increases with increasing H_2 pressure, while the percentage of W^{5+} remains almost constant. As discussed in **Section 3.2**, the higher percentage of W^{4+} could be a factor which can lower the THFDM conversion rate. The appearance of a maximum conversion rate with increasing H_2 pressure demonstrates that hydrogen can inhibit the reaction at higher hydrogen pressures indicating that high hydrogen coverages can occur on this catalyst. As shown in **Fig.S3**, the reaction is first order with respect to THDFM at 5.5 MPa H_2, indicating that THFDM does not inhibit the reaction. Thus, hydrogen can have two roles in influencing the catalyst: 1) strongly adsorbing and inhibiting the activity[59–62] and 2) reducing the W to a less active form[33].

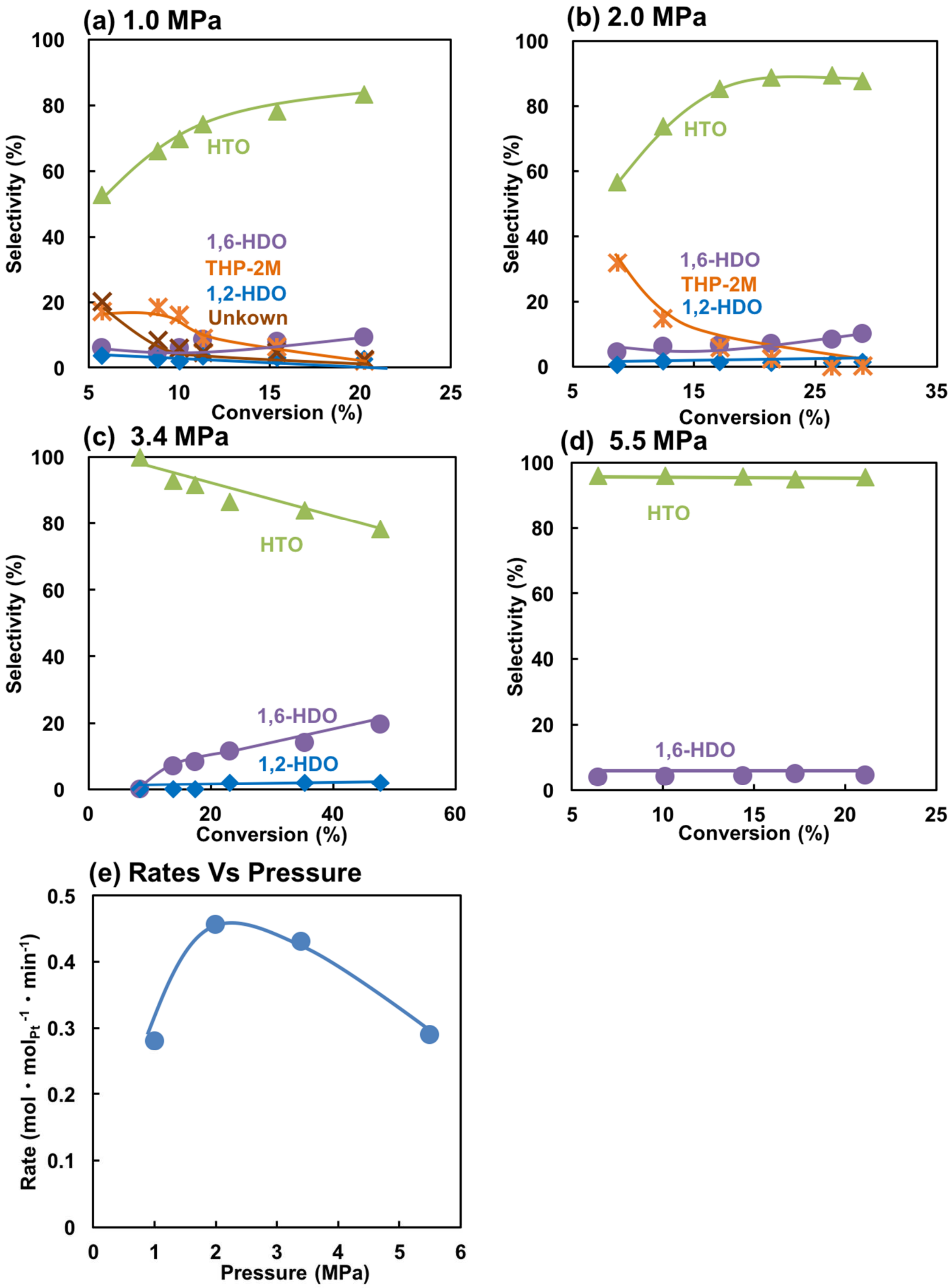

Figure 6. THFDM (5 wt% in H_2O, 20 mL) conversion and product selectivities over 10 wt% Pt-10 wt% WO_x/TiO_2 (0.10 g) catalysts at 160 °C under (a) 1.0 MPa H_2(b) 2.0 MPa H_2 (c) 3.4 MPa H_2 (d) 5.5 MPa H_2 (e) THFDM conversion rates versus reaction pressure.

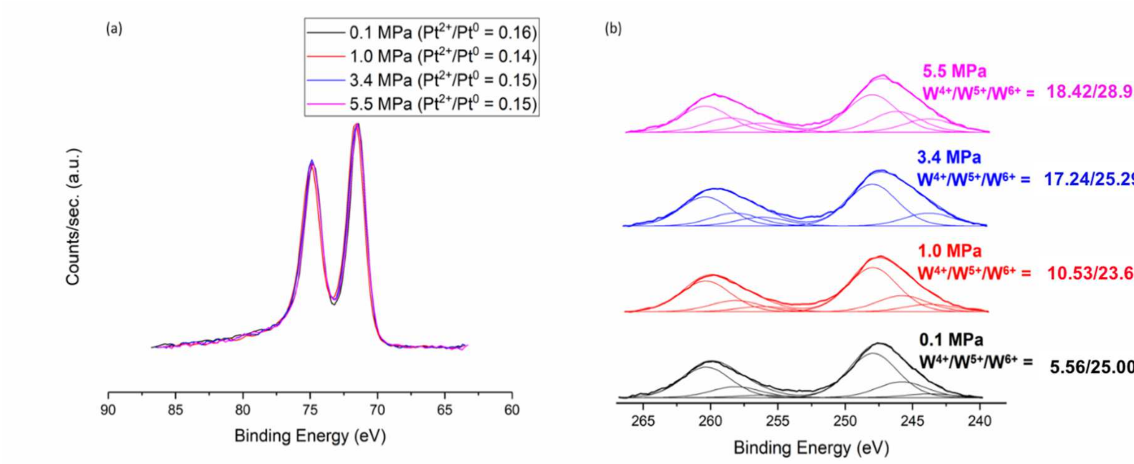

Figure 7. XPS of (a) Pt 4f and (b) W 4d regions after reduction treatments at various pressures.

3.6 THFDM conversion over Pt- WO_x/TiO_2 in a continuous flow reactor

The Pt-WO_x/TiO_2 catalyst was then studied in a fixed-bed reactor for conversion of THFDM to 1,6-HDO shown in **Figure 8**. 1,6-HDO is the main product, with selectivity increasing throughout the reaction in the range of 50-60%. The HTO selectivity increases at low times-on-stream and then stabilizes just below 30%. THP-2M is also formed with 15% selectivity at low times-on-stream. Combining selectivities to 1,6-HDO, HTO, and THP-2M, we see that the total selectivity to 1,6-HDO and its precursors exceeds 80% at each point in the reaction. Less desirable products such as 1-hexanol, 1,5-HDO, and 1,2-HDO, are also formed with < 20% combined selectivity due to the over-hydrogenolysis of 1,6-HDO and non-selective hydrogenolysis of HTO. The conversion decreases from 45% to 22% over the course of 45 hours on stream.

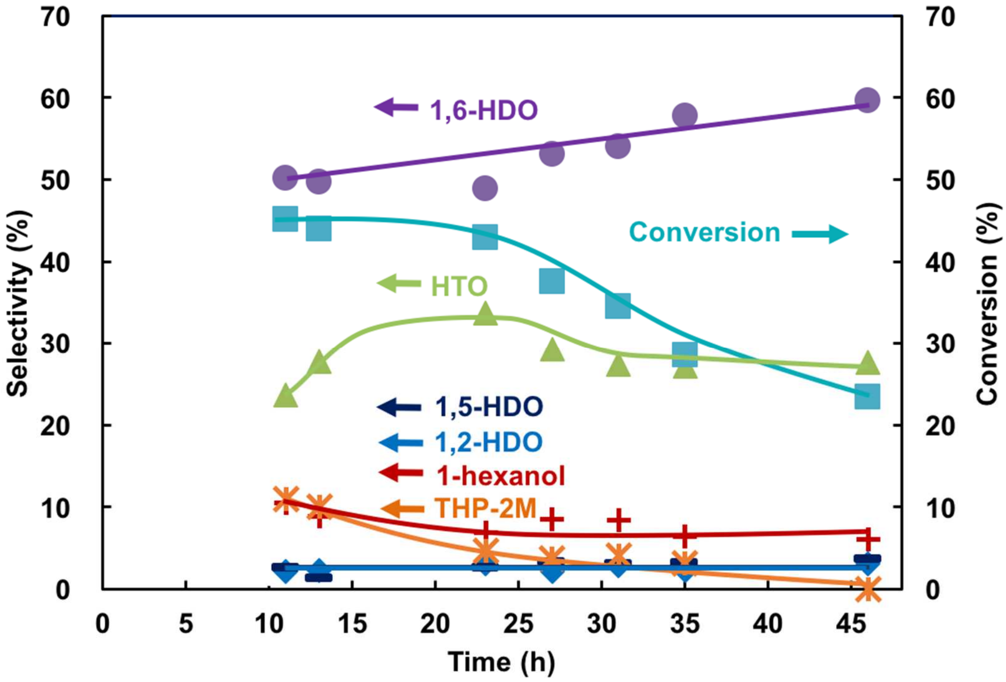

Figure 8. THFDM conversion in a continuous flow reactor. Reaction conditions: 1% aq. THFDM, 10 wt%Pt- 10 wt%WO_x/TiO_2, WHSV = 1.3 h^{-1}, 160 °C, 3.4 MPa H_2.

Tungsten was observed in the effluent liquid product. W concentrations leached in the effluent have been determined by ICP. Based on these concentrations, the remaining W in the reactor is calculated after accounting for what was detected in the effluent. The tungsten leaching rate, defined as the percentage of the initial tungsten on the catalyst that is removed each hour, as a function of time on stream (TOS) is shown in **Fig. 9**. The tungsten leaching rate decreased from 0.49 %W·h^{-1} at 11h TOS to 0.22 %W·h^{-1} at 57h, while the remaining W in the catalysts decreased from 95.3%W at 11h TOS to 79.0% at 57h. The leaching of Pt is negligible (<0.002%). It is likely that tungsten leaching is leading to the deactivation of Pt-WO_x/TiO_2, which is shown in **Fig. 8** by the decrease in conversion with increasing TOS.

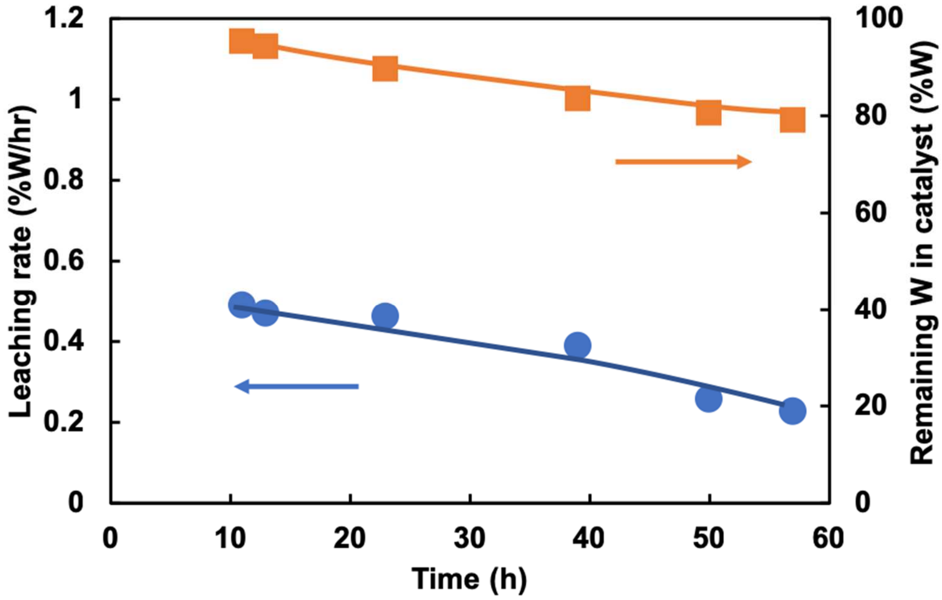

Figure 9 Tungsten leaching rate of 10 wt% Pt-10 wt% WO_x/TiO_2 in the continuous flow reactor.

3.7 THFDM hydrogenolysis with Pt/TiO_2 with homogeneous W salts

Djakovitch and Pinel *et al.* reported that the addition of W acid/salts to Rh/C greatly accelerates the glycerol conversion and selectivity to 1,3-propanediol in the glycerol hydrogenolysis in the aqueous phase under 8 MPa H_2 at 453 K [63]. To further investigate the effect of W leaching in our catalytic system and identify the extent to which the leached W contributes to the catalytic activity, we investigated the addition of homogeneous W salts to the THFDM solution. THFDM conversion rates and product selectivities over pure Pt/TiO_2 and Pt/TiO_2 with 0.029 mmol/L ammonium metatungstate (AMT) are nearly identical (**Fig. 10**), which indicates that the small amount of AMT (equivalent to 12 % of the W in 0.10 g of 10 wt% WO_x/TiO_2, which represents a much higher homogeneous W concentration than that of the leached W in 8hrs in the actual reaction, as shown in **section 3.6**) has no influence on the Pt/TiO_2 activity (**Fig. 10a and 10b**). The THFDM conversion rate increases from 0.05 $mol \cdot mol_{Pt}^{-1} \cdot min^{-1}$ with 0.029 mmol/L AMT to a maximum of 0.27 $mol \cdot mol_{Pt}^{-1} \cdot min^{-1}$ with 0.142 mmol/L AMT and then decreases to 0.14 $mol \cdot mol_{Pt}^{-1} \cdot min^{-1}$ with 0.40 mmol/L AMT (**Fig. 11**). Therefore, THFDM can be efficiently converted to HTO in the presence of Pt/TiO_2 and higher than 0.142 mmol/L of homogeneous W salts. This concentration is five times higher than what is present during leaching of Pt-WO_x/TiO_2 at conditions reported in **Fig. 8 and 9**. Therefore, we conclude that the W leached from the Pt-WO_x/TiO_2 catalyst does not contribute to the overall THFDM conversion rate.

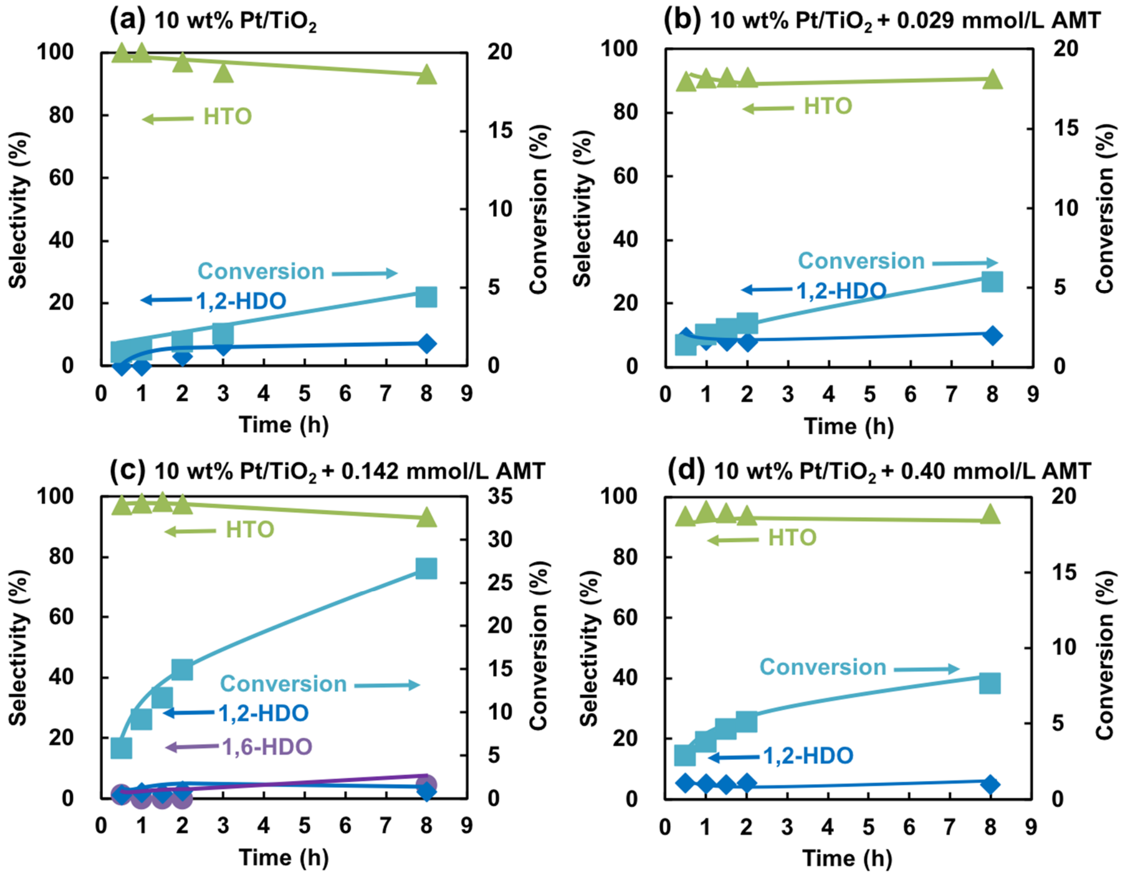

Figure 10 THFDM (5 wt% in H_2O, 20 mL) conversion over 10 wt% Pt /TiO_2 (0.10 g) catalysts and ammonia metatungstate (AMT) salts at 160 ˚C under 5.5 MPa H_2 (a) without AMT (b) with 0.029 mmol/L AMT (equivalent to 12.5% of the W of 0.10g 10 wt% WO_x/TiO_2) (c) with 0.142 mmol/L AMT (equivalent to 62% of the W of 0.10g 10 wt% WO_x/TiO_2) (d) with 0.40 mmol/L AMT (equivalent to 176% of the W of 0.10g 10 wt% WO_x/TiO_2).

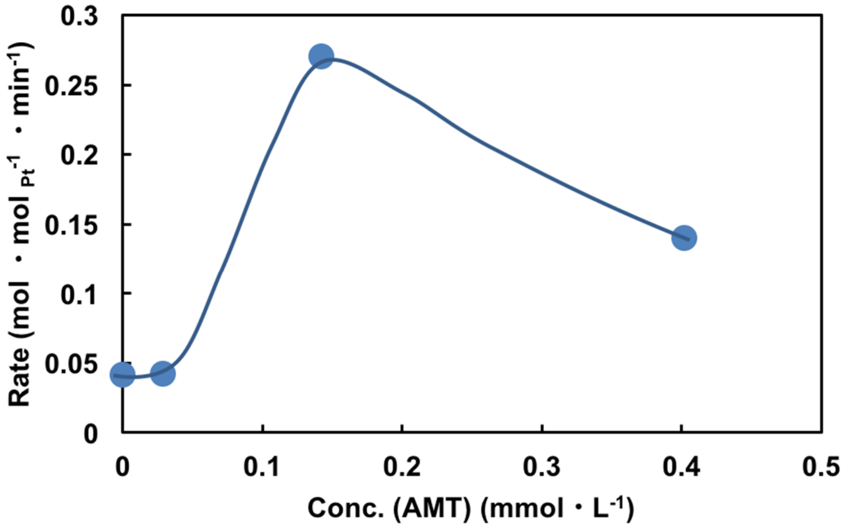

Figure 11. THFDM (5 wt% in H_2O, 20 mL) conversion rate over 10 wt% Pt /TiO_2 (0.10 g) catalysts and ammonia metatungstate (AMT) salts at 160 ˚C under 5.5 MPa H_2 THFDM conversion rates versus concentrations of ammonia metatungstate (AMT) salts.

3 Conclusions

Pt-WO_x/TiO_2 and Rh-WO_x/TiO_2 have two orders-of-magnitude higher catalytic activity (per metal site) than Ru- and Pd-WO_x/TiO_2 for THFDM hydrogenolysis. This enhanced activity is due to two effects 1) WO_x/TiO_2 overcoats Ru and Pd more than Pt and Rh, and 2) Pt and Rh are able to more effectively reduce of W^{6+} to the active W^{5+}. Pt-WO_x/TiO_2 has twice the activity (per metal site) of Rh-WO_x/TiO_2 for this reaction, even though Rh-WO_x/TiO_2 has slightly higher CO uptake. The THFDM reaction rate passes through a maximum of 0.45 $mol \cdot mol_{Pt}^{-1} \cdot min^{-1}$ with hydrogen pressure indicating that at high pressure the surface is highly covered with hydrogen. Increasing the hydrogen pressure also reduces the W oxidation state in the catalyst. In the range of 160-200 ^{o}C, we show that combined selectivity to 1,6-HDO and HTO remains above 90%. The apparent activation energy for THFDM conversion of 47 kJ mol^{-1}. The conversion decreased from 40% at 10h to 21% at 45 h over Pt-WO_x/TiO_2 under continuous-flow conditions, while selectivities to 1,6-HDO and its precursors remain high. Catalyst deactivation is likely due to tungsten leaching.

Acknowledgement

This material is based upon work supported by the Department of Energy, Office of Energy Efficiency and Renewable Energy (EERE), under Award Number DE-EE0006878. Any opinions, findings, and conclusions or recommendations expressed in this material are those of the authors and do not necessarily reflect the views of the Department of Energy. We thank Phoebe Wagner, Xiaoli Chen, Giulia Kitayama, Canhetti Mondin for assistance with THFDM and catalyst synthesis.

We also thank Lifeng Zhang for XPS measurements. The authors acknowledge use of instrumentation supported by UW MRSEC (DMR-1121288) and the UW NSEC (DMR-0832760).

Reference

[1] G.W. Huber, S. Iborra, A. Corma, Synthesis of transportation fuels from biomass: Chemistry, catalysts, and engineering, Chem. Rev. 106 (2006) 4044–4098. doi:10.1021/cr068360d.

[2] T. Werpy, G. Petersen, Top Value Added Chemicals from Biomass: Volume I- Results of Screening for potental Candidates from Sugars and Synthesis Gas, Golden, CO, 2004.

[3] G. Centi, R.A. Van Santen, Catalysis for Renewables: From Feedstock to Energy Production, 2007. doi:10.1002/9783527621118.

[4] M. De bruyn, J. Fan, V.L. Budarin, D.J. Macquarrie, L.D. Gomez, R. Simister, T.J. Farmer, W.D. Raverty, S.J. McQueen-Mason, J.H. Clark, A new perspective in bio-refining: levoglucosenone and cleaner lignin from waste biorefinery hydrolysis lignin by selective conversion of residual saccharides, Energy Environ. Sci. 9 (2016) 2571–2574. doi:10.1039/C6EE01352J.

[5] F. Cao, T.J. Schwartz, D.J. McClelland, S.H. Krishna, J.A. Dumesic, G.W. Huber, Dehydration of cellulose to levoglucosenone using polar aprotic solvents, Energy Environ. Sci. 8 (2015) 1808–1815. doi:10.1039/C5EE00353A.

[6] MarketsandMarkets, 1,6-Hexanediol Market by Application (Polyurethanes, Coatings, Acrylates, Adhesives, Unsaturated Polyester Resins, Plasticizers, and Others) - Trends and Forecasts to 2019, 2014.

[7] P. Werle, M. Morawietz, S. Lundmark, K. Sörensen, E. Karvinen, J. Lehtonen, Alcohols, Polyhydric, in: Ullmann's Encycl. Ind. Chem., 2008: pp. 263–281. doi:10.1002/14356007.a01.

[8] D.E. Mears, A.D. Eastman, Kirk-Othmer Encyclopedia of Chemical Technology, 2014.

[9] W.D. Fisher, J.F. VanPeppen, Kirk-Othmer Encyclopeida of Chemical Technology, 2000.

[10] J.P. Oppenheim, G.L. Dickerson, Kirk-Othmer Encyclopedia of Chemical Technology, 2014.

[11] K.G. Baur, R. Fischer, R. Pinkos, F. Stein, H. Rust, B. Breitscheidel, Process for preparing 1,6 hexanediol with a level of purity over 99%, US Patent US6008418A, 1999.

[12] J. He, S.P. Burt, M. Ball, D. Zhao, I. Hermans, J.A. Dumesic, G.W. Huber, Synthesis of 1,6-Hexanediol from Cellulose Derived Tetrahydrofuran-Dimethanol with Pt-WOx/TiO2Catalysts, ACS Catal. 8 (2018) 1427–1439. doi:10.1021/acscatal.7b03593.

[13] M. Faber, Process for producing adipic acid from biomass, 4,400,468, 1983.

[14] T. Buntara, S. Noel, P.H. Phua, I. Melián-Cabrera, J.G. De Vries, H.J. Heeres, Caprolactam from renewable resources: Catalytic conversion of 5-hydroxymethylfurfural into caprolactone, Angew. Chemie - Int. Ed. 50 (2011) 7083–7087. doi:10.1002/anie.201102156.

[15] T. Buntara, I. Melian-Cabrera, Q. Tan, J.L.G. Fierro, M. Neurock, J.G. De Vries, H.J. Heeres, Catalyst studies on the ring opening of tetrahydrofuran-dimethanol to 1,2,6-hexanetriol, Catal. Today. 210 (2013) 106–116. doi:10.1016/j.cattod.2013.04.012.

[16] M. Chia, Y.J. Pagán-Torres, D. Hibbitts, Q. Tan, H.N. Pham, A.K. Datye, M. Neurock, R.J. Davis, J.A. Dumesic, Selective hydrogenolysis of polyols and cyclic ethers over bifunctional surface sites on rhodium-rhenium catalysts, J. Am. Chem. Soc. 133 (2011) 12675–12689. doi:10.1021/ja2038358.

[17] K. Chen, S. Koso, T. Kubota, Y. Nakagawa, K. Tomishige, Chemoselective Hydrogenolysis

of Tetrahydropyran-2-methanol to 1,6-Hexanediol over Rhenium-Modified Carbon-Supported Rhodium Catalysts, ChemCatChem. 2 (2010) 547–555. doi:10.1002/cctc.201000018.
[18] S.P. Burt, K.J. Barnett, D.J. McClelland, P. Wolf, J.A. Dumesic, G.W. Huber, I. Hermans, Production of 1,6-hexanediol from tetrahydropyran-2-methanol by dehydration-hydration and hydrogenation, Green Chem. 19 (2017) 1390–1398. doi:10.1039/c6gc03606f.
[19] A.M. Allgeier, W.I.N. De Silva, E. Korovessi, C.A. Menning, J.C. Ritter, S.K. Sengupta, C.S. Stauffer, Process for preparing 1,6-hexanediol, 2014.
[20] V. Sokolovskii, M. Lavrenko, A. Hagemeyer, E. Dias, J.A. Shoemaker, V.J. Murphy, Process for production of hexanetriol from 5-Hydroxymethylfurfural, US 9,586,920 B2, 2017.
[21] W. Karim, C. Spreafico, A. Kleibert, J. Gobrecht, J. VandeVondele, Y. Ekinci, J.A. van Bokhoven, Catalyst support effects on hydrogen spillover, Nature. 541 (2017) 68–71. doi:10.1038/nature20782.
[22] P. Frediani, U. Matteoli, M. Bianchi, F. Piacenti, G. Menchi, Cluster ruthenium hydrogenation catalysts, J. Organomet. Chem. 150 (1978) 273–278. doi:10.1016/S0022-328X(00)84730-0.
[23] J.M. Tour, J.P. Cooper, S.L. Pendalwar, Highly selective heterogeneous palladium-catalyzed hydrogenations using triethoxysilane and water, J. Org. Chem. 55 (1990) 3452–3453.
[24] W.S. Knowles, Asymmetric Hydrogenations, Angew. Chemie - Int. Ed. 41 (2002) 1998–2007.
[25] D.M. Alonso, S. Hakim, S. Zhou, W. Won, O. Hosseinaei, J. Tao, V. Garcia-Negron, A.H. Motagamwala, M.A. Mellmer, K. Huang, C.J. Houtman, N. Labbé, D.P. Harper, C. Maravelias, T. Runge, J.A. Dumesic, Increasing the revenue from lignocellulosic biomass: Maximizing feedstock utilization, ScienceAdvances. (2017). doi:10.1126/sciadv.1603301.
[26] J. He, M. Liu, K. Huang, T.W. Walker, C.T. Maravelias, J.A. Dumesic, G.W. Huber, Production of levoglucosenone and 5-hydroxymethylfurfural from cellulose in polar aprotic solvent–water mixtures, Green Chem. 19 (2017) 3642–3653. doi:10.1039/C7GC01688C.
[27] S.H. Krishna, D.J. McClelland, Q.A. Rashke, J.A. Dumesic, G.W. Huber, Hydrogenation of levoglucosenone to renewable chemicals, Green Chem. 19 (2017) 1278–1285. doi:10.1039/C6GC03028A.
[28] J. He, K. Huang, K.J. Barnett, S. Krishna, D.M. Alonso, Z.J. Brentzel, S.P. Burt, T. Walker, W.F. Banholzer, C.T. Maravelias, I. Hermans, J.A. Dumesic, G.W. Huber, New catalytic strategies for α,ω-diols production from lignocellulosic biomass, Faraday Discuss. 202 (2017) 247–267. doi:10.1039/C7FD00036G.
[29] S.H. Krishna, K. Huang, K.J. Barnett, J. He, C.T. Maravelias, J.A. Dumesic, G.W. Huber, M. De bruyn, B.M. Weckhuysen, Oxygenated commodity chemicals from chemo-catalytic conversion of biomass derived heterocycles, AIChE J. 64 (2018) 1910–1922. doi:10.1002/aic.16172.
[30] Y. Amada, Y. Shinmi, S. Koso, T. Kubota, Y. Nakagawa, K. Tomishige, Reaction mechanism of the glycerol hydrogenolysis to 1,3-propanediol over Ir-ReOx/SiO2 catalyst, Appl. Catal. B Environ. 105 (2011) 117–127. doi:10.1016/j.apcatb.2011.04.001.
[31] K. Tomishige, Y. Nakagawa, M. Tamura, metal catalysts directly modified with metal oxide, Green Chem. 19 (2017) 2876–2924. doi:10.1039/c7gc00620a.
[32] P.U. Karanjkar, S.P. Burt, X. Chen, K.J. Barnett, M.R. Ball, M.D. Kumbhalkar, X. Wang,

J.B. Miller, I. Hermans, J.A. Dumesic, G.W. Huber, Effect of carbon supports on RhRe bifunctional catalysts for selective hydrogenolysis of tetrahydropyran-2-methanol, Catal. Sci. Technol. 6 (2016) 7841–7851. doi:10.1039/c6cy01763k.
[33] J. Wang, X. Zhao, N. Lei, L. Li, L. Zhang, S. Xu, S. Miao, X. Pan, A. Wang, T. Zhang, Hydrogenolysis of Glycerol to 1,3-propanediol under Low Hydrogen Pressure over WOx-Supported Single/Pseudo-Single Atom Pt Catalyst, ChemSusChem. 9 (2016) 784–790. doi:10.1002/cssc.201501506.
[34] S. García-Fernández, I. Gandarias, J. Requies, M.B. Güemez, S. Bennici, A. Auroux, P.L. Arias, New approaches to the Pt/WOx/Al2O3 catalytic system behavior for the selective glycerol hydrogenolysis to 1,3-propanediol, J. Catal. 323 (2015) 65–75. doi:10.1016/j.jcat.2014.12.028.
[35] S. Zhu, X. Gao, Y. Zhu, J. Cui, H. Zheng, Y. Li, SiO2 promoted Pt/WOx/ZrO2 catalysts for the selective hydrogenolysis of glycerol to 1,3-propanediol, Appl. Catal. B Environ. 158–159 (2014) 391–399. doi:10.1016/j.apcatb.2014.04.049.
[36] J. Sá, J. Bernardi, J.A. Anderson, Imaging of low temperature induced SMSI on Pd/TiO2 catalysts, Catal. Letters. 114 (2007) 91–95. doi:10.1007/s10562-007-9049-1.
[37] X. Shen, L.-J. Garces, Y. Ding, K. Laubernds, R.P. Zerger, M. Aindow, E.J. Neth, S.L. Suib, Behavior of H2 chemisorption on Ru/TiO2 surface and its application in evaluation of Ru particle sizes compared with TEM and XRD analyses, Appl. Catal. A Gen. 335 (2008) 187–195. doi:10.1016/j.apcata.2007.11.017.
[38] Y.V. Larichev, O.V. Netskina, O.V. Komova, V.I. Simagina, Comparative XPS study of Rh/Al2O3 and Rh/TiO2 as catalysts for NaBH4 hydrolysis, Int. J. Hydrogen Energy. 35 (2010) 6501–6507. doi:10.1016/j.ijhydene.2010.04.048.
[39] M. Englisch, A. Jentys, J.A. Lercher, Structure Sensitivity of the Hydrogenation of Crotonaldehyde over Pt/SiO2and Pt/TiO2, J. Catal. 166 (1997) 25–35. doi:10.1006/jcat.1997.1494.
[40] L. Jiao, J.R. Regalbuto, The synthesis of highly dispersed noble and base metals on silica via strong electrostatic adsorption: I. Amorphous silica, J. Catal. 260 (2008) 329–341. doi:10.1016/j.jcat.2008.09.022.
[41] S.J. Tauster, S.C. Fung, R.L. Garten, Strong Metal-Support Interactions. Group 8 Noble Metals Supported on TiO2, J. Am. Chem. Soc. 100 (1978) 170–175. doi:10.1021/ja00469a029.
[42] G.L. Haller, D.E. Resasco, Metal–Support Interaction: Group VIII Metals and Reducible Oxides, Adv. Catal. 36 (1989) 173–235. doi:10.1016/S0360-0564(08)60018-8.
[43] J.D. Bracey, R. Burch, Enhanced activity of Pd TiO2 catalysts for the CO H2 reaction in the absence of strong metal-support interactions (SMSI), J. Catal. 86 (1984) 384–391. doi:10.1016/0021-9517(84)90383-X.
[44] M.S. Spencer, Models of strong metal-support interaction (SMSI) in Pt on TiO2 catalysts, J. Catal. 93 (1985) 216–223. doi:10.1016/0021-9517(85)90169-1.
[45] Tauster S.J., Strong Metal Support Interaction., Acc. Chem. Res. 20 (1987) 389–394. doi:10.1016/B978-0-444-81468-5.50015-7.
[46] S. Zhang, P.N. Plessow, J.J. Willis, S. Dai, M. Xu, G.W. Graham, M. Cargnello, F. Abild-Pedersen, X. Pan, Dynamical observation and detailed description of catalysts under strong metal-support interaction, Nano Lett. 16 (2016) 4528–4534. doi:10.1021/acs.nanolett.6b01769.
[47] A. David Logan, E.J. Braunschweig, A.K. Datye, D.J. Smith, Direct Observation of the

Surfaces of Small Metal Crystallites: Rhodium Supported on TiO2, Langmuir. 4 (1988) 827–830. doi:10.1021/la00082a009.
[48] A.K. Datye, D.S. Kalakkad, M.H. Yao, D.J. Smith, Comparison of Metal-Support Interactions in Pt_TiO2 and Pt_CeO2 J Catal 1995, J. Catal. 155 (1995) 148–153. doi:10.1006/jcat.1995.1196.
[49] J. Liu, Advanced Electron Microscopy Characterization of Nanostructured Heterogeneous Catalysts, Microsc. Microanal. 10 (2004) 55–76. doi:10.1017/S1431927604040310.
[50] J. Goralski, V.S. Federyaeva, R.F. Vitkovskaya, M. Szinkowska, Study of properties of Al2O3 and TiO2 supported palladium catalysts in reactions of tetrachloromethane hydrogenation, Russ. J. Appl. Chem. 85 (2012) 598–603. doi:10.1134/S1070427212040118.
[51] H. Zhu, Z. Qin, W. Shan, W. Shen, J. Wang, Pd/CeO2-TiO2 catalyst for CO oxidation at low temperature: A TPR study with H2 and CO as reducing agents, J. Catal. 225 (2004) 267–277. doi:10.1016/j.jcat.2004.04.006.
[52] D. Li, N. Ichikuni, S. Shimazu, T. Uematsu, Hydrogenation of CO_2 over sprayed Ru/TiO_2 fine particles and strong metal–support interaction, Appl. Catal. A Gen. 180 (1999) 227–235. doi:10.1016/S0926-860X(98)00335-4.
[53] D.J. Morgan, Resolving ruthenium: XPS studies of common ruthenium materials, Surf. Interface Anal. 47 (2015) 1072–1079. doi:10.1002/sia.5852.
[54] C. Elmasides, D.I. Kondarides, W. Gru, X.E. Verykios, XPS and FTIR Study of Ru / Al2O3 and Ru / TiO2 Catalysts : Reduction Characteristics and Interaction with a Methane - Oxygen Mixture, J. Phys. Chem. B. 3 (1999) 5227–5239.
[55] G. Bergeret, P. Gallezot, Particle Size and Dispersion Measurements, in: G. Ertl, H. Knozinger, J. Weitkamp (Eds.), Handb. Heterog. Catal., 2nd ed., VCH Verlagsgesellschaft mbH, Weinheim, 1997: pp. 439–441. doi:10.1002/9783527619474.ch3a.
[56] D.D. Sarma, C.N.R. Rao, XPES studies of oxides of second- and third-row transition metals including rare earths, J. Electron Spectros. Relat. Phenomena. 20 (1980) 25–45. doi:10.1016/0368-2048(80)85003-1.
[57] J.E. Benson, H.W. Kohn, M. Boudart, On the reduction of tungsten trioxide accelerated by platinum and water, J. Catal. 5 (1966) 307–313.
[58] R.B. Levy, M. Boudart, The kinetics and mechanism of spillover, J. Catal. 32 (1974) 304–314.
[59] J. He, C. Zhao, J.A. Lercher, Ni-catalyzed cleavage of aryl ethers in the aqueous phase, J. Am. Chem. Soc. 134 (2012) 20768–20775. doi:10.1021/ja309915e.
[60] J. He, C. Zhao, D. Mei, J.A. Lercher, Mechanisms of selective cleavage of C-O bonds in di-aryl ethers in aqueous phase, J. Catal. 309 (2014) 280–290. doi:10.1016/j.jcat.2013.09.012.
[61] J. He, L. Lu, C. Zhao, D. Mei, J.A. Lercher, Mechanisms of catalytic cleavage of benzyl phenyl ether in aqueous and apolar phases, J. Catal. 311 (2014) 41–51. doi:10.1016/j.jcat.2013.10.024.
[62] J. He, C. Zhao, J.A. Lercher, Impact of solvent for individual steps of phenol hydrodeoxygenation with Pd/C and HZSM-5 as catalysts, J. Catal. 309 (2014) 362–375. doi:10.1016/j.jcat.2013.09.009.
[63] J. Chaminand, L. Djakovitch, P. Gallezot, P. Marion, C. Pinel, C. Rosier, Glycerol hydrogenolysis on heterogeneous catalysts, Green Chem. 6 (2004) 359–361. doi:10.1039/c7gc00620a.

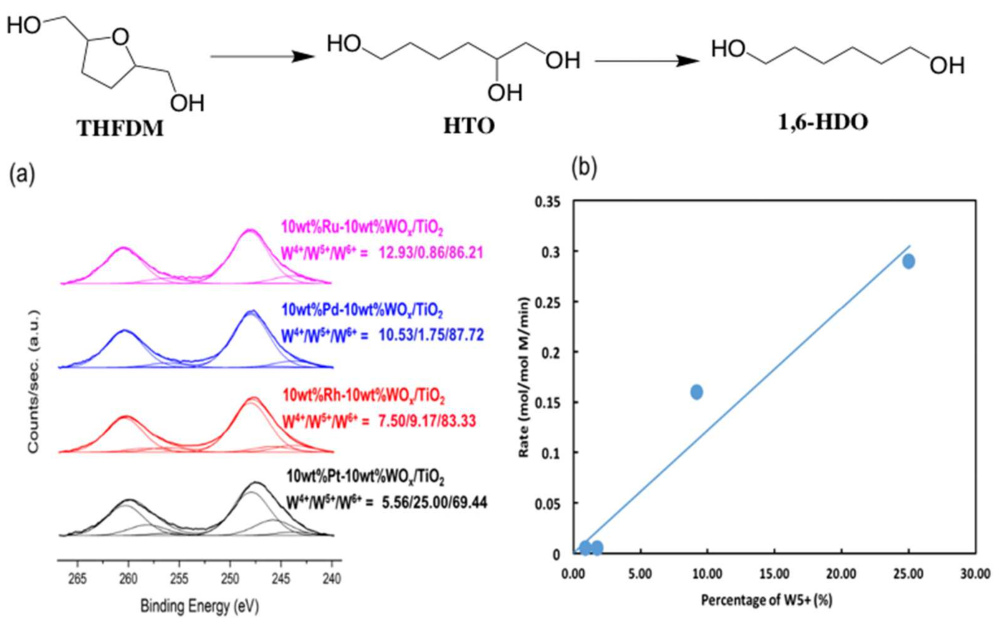

HO
O
OH
THFDM
HO
OH
OH
HTO
HO
OH
1,6-HDO
(a)
10wt%Ru-10wt%WOx/TiO2
W4+/W5+/W6+ = 12.93/0.86/86.21
10wt%Pd-10wt%WOx/TiO2
W4+/W5+/W6+ = 10.53/1.75/87.72
10wt%Rh-10wt%WOx/TiO2
W4+/W5+/W6+ = 7.50/9.17/83.33
10wt%Pt-10wt%WOx/TiO2
W4+/W5+/W6+ = 5.56/25.00/69.44
Counts/sec. (a.u.)
Binding Energy (eV)
265 260 255 250 245 240
(b)
Rate (mol/mol M/min)
Percentage of W5+ (%)
0 0.05 0.1 0.15 0.2 0.25 0.3 0.35
0.00 5.00 10.00 15.00 20.00 25.00 30.00